Eng. Sci., 2021, **13**, 106–120

Engineered Science

DOI: https://dx.doi.org/10.30919/es8d1159

Microencapsulation of Poorly Water-soluble Finasteride in Polyvinyl Alcohol/chitosan Microspheres as a Long-term Sustained Release System for Potential Embolization Applications

Xiaohong Li,[1] Kun Chen,[1] Xiongfa Ji,[2] Xi Yuan,[3] Zehua Lei,[3] Muhammad Wajid Ullah,[1,*] Jun Xiao[3,*] and Guang Yang[1,*]

Abstract

Prostatic artery embolization (PAE) has been widely applied as an alternative option to treat symptomatic benign prostatic hyperplasia (BPH). However, hitherto, very few drug-loaded embolic materials have been developed to improve the therapeutic efficacy of PAE. In this study, the poorly water-soluble finasteride (FNS) was micronized *via* a homogenization technique in the presence of a hydrophilic surfactant, followed by encapsulating the crystalline FNS dispersion in polyvinyl alcohol/chitosan (PVA/CS) matrix *via* emulsification crosslinking method. The prepared FNS-loaded PVA/CS microspheres (FNS@PVA/CS MS) were characterized for their physicochemical properties. Results showed that the MS were well-dispersed and spherical, with an average particle size of 191.5 μm. The FNS was presented in crystalline form inside the MS, which exhibited controlled and sustained release of FNS up to 45 days. *In vitro* biocompatibility evaluations indicated that the MS were non-cytotoxic and hemocompatible. Moreover, *in vivo* transauricular embolization studies in rabbits revealed the effective occlusion of the MS in the auricular central arteries, and exhibited superior embolization effects. Furthermore, the persistent embolization resulted in prominent ultrastructural alternations of endothelial cells in ischemic necrosis region. These results suggest that the drug-delivering MS could be a promising embolic agent for BPH therapy.

Keywords: Benign prostatic hyperplasia; Hydrophobic drug; Homogenization; Wetting; Polyvinyl alcohol/chitosan.
Received: 10 November 2020; Accepted: 14 December 2020.
Article type: Research article.

1. Introduction

Benign prostatic hyperplasia (BPH), typically associated with a high risk of severe voiding symptoms in patients, has a prevalence among men over 50 years and further becomes severe with age.[1,2] Prostatic artery embolization (PAE), an emerging minimally-invasive treatment, has emerged as a safe and effective procedure to reduce the severity of urinary retention symptoms caused by BPH.[3, 4] The PAE is interpreted as the intravascular injection of embolic agents to block the prostatic artery, and subsequently prevents the blood supply to the prostate gland, thus resulting in a reduction of prostate volume and relief in BPH symptoms.[5, 6] Previous studies have demonstrated that the microspheres (MS) with regular shape and smooth surface are advantageous as compared to the non-spherical particles regarding their catheter deliverability and devascularization ability.[7-9] Over the past few years, the embolic drug-eluting MS have been introduced in an attempt to improve the embolization efficacy.[10] To date, two types of drug-loaded MS, namely, the DC Bead (Biocompatibles, UK) and HepaSphere MS (BioSphere Medical, USA), have been extensively used clinically in transcatheter arterial chemoembolization (TACE), in which the anticancer drug such as doxorubicin (DOX) and epirubicin can be loaded into the beads through drug-bead ionic interactions.[11-14] Therefore, the drug-eluting MS could deliver the drug in a controlled

[1] *Department of Biomedical Engineering, College of Life Science and Technology, Huazhong University of Science and Technology, Wuhan 430074, China.*
[2] *Department of Orthopedics, Guangdong Provincial People's Hospital, Guangdong Academy of Medical Sciences, Guangzhou 510080, China.*
[3] *Department of Orthopaedics, Tongji Hospital, Tongji Medical College, Huazhong University of Science and Technology, Wuhan 430030, China.*
[*] *Email:* yang_sunny@yahoo.com (G. Yang); jun_xiao@hust.edu.cn (J. Xiao); wajid_kundi@hust.edu.cn (M. Wajid Ullah)

manner, and obtain higher drug concentrations in the tumor bed, with fewer toxicity events compared to the conventional TACE.[15-16] To the authors' knowledge, only a few drug-loaded embolization systems have been developed for BPH therapy. Consequently, it is in high demand of developing drug-loaded embolic agents that can achieve the blood vessel occlusion and simultaneously deliver the drug locally when managing BPH.

Among various available polymeric MS designed for embolization applications, polyvinyl alcohol (PVA) MS is one of the most widely used embolic agent used for PAE applications due to its safe and effective performance in the clinical practice.[17-19] Nevertheless, hitherto, few studies are available on the use of PVA MS to directly load BPH therapeutic drugs as the controlled drug delivery devices, which hinders the development in the management of BPH.

Finasteride (FNS), a chemically synthetic 4-azasteroid drug, has been introduced as an effective oral therapeutic agent to treat BPH and male pattern baldness.[20-21] It is considered as the first competitive 5α-reductase inhibitor that prevents testosterone from converting to more potent dihydrotestosterone,[22] thereby reducing the prostate size and alleviating the acute urinary obstruction symptoms. However, the oral administration of FNS is associated with systematic side effects, including mood disturbance, gynaecomastia, decreased libido, erectile dysfunction, and ejaculation disorder.[23] In addition, the extremely low solubility of FNS in aqueous solution limits its bioavailability and clinical efficacy, which also poses a major hurdle in designing FNS-loaded PVA MS. To address this issue, a multicore-shell drug delivery system was developed in our previous study,[24] in which the FNS-loaded polyhydroxybutyrate valerate (PHBV) MS were first fabricated and then embedded in a PVA/chitosan (PVA/CS) MS matrix. Although it is an effective strategy, the preparation process is overly complicated and resulted in low drug loading in the hybrid MS. Therefore, it is desirable to employ a single-step method for the preparation of FNS-loaded PVA/CS (FNS@PVA/CS) MS with high drug loading capability. According to previous studies, there are several methods that are available to improve the solubility of the drug in an immiscible matrix.[25] One common strategy is to increase the specific surface area by milling the large drug crystals into smaller sizes. The high-pressure homogenization, as one of the alternative break-down methods, has been used to prepare nanonized or micronized drug crystals.[26, 27] Previously, Kluge *et al*. applied the high-pressure homogenization to comminute the pharmaceutical solids by adjusting the parameters of pressure drop and the number of passes across the homogenizer, which showed that the increase in homogenization pressure or the number of passes resulted in smaller particle sizes.[28] Kamiya *et al*. obtained the nifedipine (IB) and griseofulvin (GF) nanoparticles with approximately 50 nm by employing a combination of roll mill and high-pressure homogenization.[29] Another alternative to enhance the solubility of poorly water-soluble drug is to incorporate a small amount of surfactant,[30] as such, the poorly water-soluble drug would remain in dispersed form due to the improved particle wetting.[31]

In the present study, we encapsulated the poorly water-soluble FNS into the hydrophilic PVA/CS polymeric MS through a modified inverse emulsification crosslinking method. A small amount of CS was added in the PVA polymeric matrix to prevent the agglomeration of MS in that the positively charged CS in acidic conditions would endow them with repulsive forces. Specifically, the high-pressure homogenization method combined with the inclusion of a surfactant was first used to develop a stabilized drug crystal suspension, followed by dispersion in PVA/CS polymeric matrix to prepare FNS@PVA/CS MS *via* an emulsification crosslinking method. The prepared FNS@PVA/CS MS were characterized for their surface and cross-sectional morphology, particle size, chemical structures, and thermal stability. The MS were further evaluated for the drug release profile, cytotoxicity, and hemocompatibility. Furthermore, the endovascular embolization performance of the MS was investigated by conducting the embolization on the auricular central arteries in rabbits.

2. Experimental section

2.1 Materials

Polyvinyl alcohol (PVA-124, Mw~105 kDa, degree of hydrolysis 98.0-99.8 mol%) was provided by the Shnopharm Chemical Reagent Co., Ltd. (China). Poly (vinyl alcohol) (PVA-1788, Mw: 72.6-81.4 kDa, hydrolysis 87-89 mol%) was obtained from Aladdin Reagent Co., Ltd. (China). Chitosan (CS, Mw: 110-150 kDa, deacetylation degree: 93%) was purchased from Sigma-Aldrich (USA). Finasteride (FNS, purity: > 99%) was produced by Dalian Meilun Biotechnology Co., Ltd. (China). Fetal bovine serum (FBS), DMEM medium, and penicillin-streptomycin combination were received from Gibco Life Technologies Co. Ltd. (Grand Island, USA). Cell Counting Kit-8 (CCK-8) assay was provided by Dojindo Laboratories (Japan). All other chemicals and reagents obtained from commercial suppliers were of analytical grade and used without further purification.

The New Zealand white rabbits were used as experimental animal models in this study, which were bought from the Experimental Animal Center of the affiliated hospital in our institution. The *in vivo* auricular embolization was complied with the regulations made by the Research Animal Ethical Committee of our hospital.

2.2 Preparation of FNS@PVA/CS MS

FNS@PVA/CS MS were prepared by the modified solid-in-water-in-oil (S/W/O) emulsification crosslinking method. Briefly, a 0.1 g of CS was accurately weighed and added to 10 mL of acetic acid (1 wt%), the mixture was stirred continuously in a water bath (50 ºC) to obtain the 1% (w/v) CS solution. The 13.7 wt% PVA solution was prepared by

dissolving 1.35 g of PVA124 in 8.5 mL of distilled water (85 ºC) with vigorous stirring. Thereafter, the PVA and CS solutions were blended at an appropriate proportion of 19:1 (PVA:CS, w/w), with vigorous stirring to form a homogeneous mixture of 7.2% (w/v) PVA/CS solution. Prior to preparing the drug-loaded PVA/CS MS, 200 mg of FNS was added in 3 mL of 0.5% (w/v) PVA1788 solution, and homogenized at 10000 rpm for 4 min. Subsequently, the resulting FNS dispersion was added dropwise to the PVA/CS solution, with the drug to PVA/CS at a weight ratio of 20:80. This drug/polymer mixture was stirred for 30 min at 1000 rpm until the homogenous white suspension was obtained, and then subjected to sonication for 30 min. The drug-loaded blend polymer aqueous solution was dispersed slowly into the oil phase comprised of 72 mL of n-heptane and 2.5% (w/v) Span80, and stirred at 500 rpm to form an S/W/O emulsion. After 30 min, the mixed solution of 2.6 mL of 25 wt% glutaraldehyde (GA) and 4.15 mL of diethyl ether was rapidly dropped to the emulsion. After a 5 min equilibration, a small amount of HCl (catalyst) was introduced to accelerate the crosslinking. The temperature of the emulsion was gradually increased to 55 ºC and further stirred for 5 h. The formed MS were first rinsed with petroleum ether, then several times with ethanol and distilled water. Next, a 4 wt% glycine solution was used to remove the residual crosslinking agent and vacuum-dried. The same protocol was used to prepare PVA/CS MS as a control. The MS with particle size of 100 to 300 μm for the following experiments were obtained by sieving the FNS@PVA/CS and PVA/CS MS using the standard sieves.

2.3 Characterization

The surface and cross-sectional structures of drug-free and drug-loaded PVA/CS MS, and pure drug were examined by FESEM (Sirion 200, FEI, Holland). The samples were vacuum-coated with a thin layer of gold, and then observed at a working voltage of 10 kV. The mean particle size was analyzed by measuring 100 MS at least eight different fields of view, using ImageJ 1.40 g software (NIH, Maryland, USA). The chemical compositions of the MS and FNS were analyzed by Vertex-70 FTIR spectrometer (Bruker Optics, Ettlingen, Germany) using a KBr pellet method. The FTIR spectra were recorded ranging from 4000 to 400 cm^{-1} with a resolution of 2 cm^{-1}. The crystalline structures of the samples were assessed by an X-ray diffractometer (XRD, Empyrean, PANalytical, Holland) operated at 40 V and 40 mA. The XRD patterns were collected from 5 to 60º at 8 º/min. The thermal properties of the samples were analyzed on a thermogravimetric analyzer (TGA, Pyrisl, Perkin Elmer, China), which heated from 30 to 600 ºC at a heating rate of 10 ºC/min, using pure N_2 as the protective atmosphere.

2.4 Determination of drug loading and encapsulation efficiency of FNS@PVA/CS MS

The amount of FNS encapsulated within the MS was determined by an extraction method, according to a previous study with some modifications.[32] Briefly, the FNS@PVA/CS MS were first crushed into powder, and then accurately weighed 20 mg of the MS powder into a vial containing 5 mL of DCM. The vial was then transferred to a water bath (37 ºC), and the same volume of methanol was added. After being vortexed for 5 min, the MS powder dispersion was centrifuged to separate the upper phase containing the free drug. To allow the drug to be extracted adequately from the MS powder, this process was repeated for more than three times and the methanol extracts were combined. Finally, the amount of the drug in the collected supernatant was determined using high-performance liquid chromatography (HPLC) (Shimadzu Corporation, Japan) consisted of a UV-vis detector (SPD-10A VP Plus) and LC workstation (CBM-10A VP Plus). The collected extracts were filtered through 0.45 μm nylon membrane filters, and 20 μL of the extract was injected for HPLC measurement. The chromatographic separation proceeded on the Hypersil ODS2 C18 analytical column (4.6 mm × 250 mm, 5 μm) manufactured by Dalian Elite Analytical Instruments. An acetonitrile-water (60:40, v/v) mobile phase was used in HPLC to separate FNS from the extracts, and detected at a wavelength of 210 nm. The mobile phase was flowed at 1.0 mL/min· throughout the detection. The drug loading (DL) and encapsulation efficiency (EE) were determined according to Eq. (1) and (2), respectively.

$$\text{DL (\%)} = \frac{\text{Amount of FNS measured in MS}}{\text{Amount of MS used for extraction}} \times 100 \quad (1)$$

$$\text{EE (\%)} = \frac{\text{Amount of FNS measured in MS}}{\text{Amount of FNS initially added to the formulation}} \times 100 \quad (2)$$

2.5 *In vitro* drug release studies

The FNS release studies were performed at 37 ºC in PBS buffer containing 0.1% (w/v) Tween80. The addition of Tween80 in PBS was used to enhance the solubility of poorly water-soluble FNS in the release medium. An accurately weighed 10 mg of FNS and FNS@PVA/CS MS (containing an equal amount of FNS encapsulated) were placed into a 3.5 kDa MWCO dialysis bag containing 5 mL of PBS, and then added to a vial filled with 35 mL of PBS. At regular time points, an aliquot of 2 mL of release medium was absorbed and replenished with the same volume of PBS. The concentration of FNS at different time intervals was determined by HPLC as described in Section 2.4. All release experiments were conducted in triplicate. Finally, the morphology of the MS after drug release was examined by FESEM.

2.6 Cytocompatibility evaluation of drug-free and drug-loaded PVA/CS MS

The cell viability of the drug-free and drug-loaded PVA/CS MS against HVSMCs was evaluated by CCK-8 assays using an indirect contact method. Briefly, the extract samples were obtained by incubating the MS in DMEM culture medium (10% FBS and 1% penicillin-streptomycin) at 37 ºC for 24 h. HVSMCs were seeded in 96-well plates (5×10^3 cells/well) containing 200 μL of DMEM culture medium and incubated

at 37 ºC, 5% CO_2 for 24 h. Following that, the cells were rinsed with PBS and replaced with the same volume of extracts. At 24, 48, and 72 h, the medium was aspirated out and rinsed twice with PBS. The CCK-8 working solution (CCK-8:DMEM = 1:9, v/v) was added to the plates and incubated for another 1 h at 37 ºC. The absorbance of each well was measured at a wavelength of 450 nm by using a 96-well Multiskan EX microplate reader (Thermo Fisher Scientific, USA). The cells cultured with DMEM were used as the negative control, while 0.64% (w/v) phenol contained in the culture medium was used as the positive control, respectively. The cell viability was calculated relative to the negative control group. Each sample was measured in triplicate from the independent experiments.

The Live/Dead assay was performed to determine the cytotoxicity of MS (10 mg/mL) on HVSMCs. Briefly, the MS were co-cultured with HVSMCs (5×10^4 cells/well) in a 24-well plate. The culture medium containing 0.64% (w/v) phenol and pure culture medium were designated as the positive and negative control, respectively. After 24 and 72 h of incubation, the cells were rinsed twice with PBS. Afterward, the cells were incubated with the fluorescence working solution containing 2 µM Calcein-AM and 4 µM PI (Dojindo Laboratories, Kyushu, Japan) at 37 ºC for 15 min, followed by visualization using CLSM (Olympus FV1000, Japan).

The cell morphology on the MS was studied after incubation for 24 and 72 h. The cell-MS constructs were fixed in 2.5 wt% GA at 4 ºC overnight, rinsed with PBS sufficiently, and then dehydrated consecutively in ascending concentrations of ethanol (50%, 60%, 70%, 90%, 95%, and 100%). Following that, the cell-MS constructs were allowed to dry in the air, mounted on the aluminum stubs, and vacuum-coated with gold for 150 s before observation using FESEM at 10 kV.

2.7 Hemocompatibility analysis of drug-free and drug-loaded PVA/CS MS

The hemolytic potential of the MS was assessed according to an earlier reported method.[33] Prior to testing, 10 mg of drug-free and drug-loaded PVA/CS MS were placed into a tube filled with 5 mL of normal saline, then allowed to equilibrate at 37 ºC for 1 h. Subsequently, 100 µL of the anticoagulant New Zealand white rabbit blood (4 mL of fresh blood diluted by the addition of 5 mL of normal saline) was added to the samples. The samples were incubated at 37 ºC for another 1 h. Then, the supernatant of each group was collected after centrifugation at 250 g for 10 min, and measured at a wavelength of 545 nm using a UV-vis spectrophotometer (Cary 100 bio, Varian). Accordingly, normal saline and distilled water were set as the negative and positive control, respectively. All experiments were performed in triplicate. The hemolysis ratio (HR) was calculated according to Eq. (3).

$$HR\ (\%) = \frac{OD_t - OD_n}{OD_p - OD_n} \times 100 \quad (3)$$

where OD_t, OD_n, and OD_p are the absorbance of the tested samples, negative control, and positive control, respectively.

The protocol used to evaluate the platelet adhesion and morphology on the MS was derived from a previous study.[34] Briefly, the fresh blood from a New Zealand white rabbit was centrifuged at 250 g for 15 min to obtain the platelet-rich plasma (PRP). Then, 10 mg of the MS was added to a tube and incubated with 400 µL of PRP at 37 ºC for 1 h. The glass MS (177-250 µm, AS ONE, Osaka, Japan) were used as the control in this study. After that, the MS were rinsed with saline solution to remove the unadhered platelets, while the adhered platelets were fixed with 2.5 wt% GA and rinsed thoroughly with saline to remove the residual GA. The MS were followed by dehydration with an ascending concentration of graded ethanol (30%, 50%, 70%, 80%, 90%, 95%, and 100%). Finally, the adherence of platelets on the MS surface was visualized under FESEM after vacuum-coated with a gold layer.

2.8 Auricular central artery embolization experiments of MS in rabbits

The auricular central artery embolization was carried out according to an established protocol.[35] Briefly, the rabbits were anesthetized with an administration of 30 mg/kg pentobarbital sodium from the marginal ear vein. The fur on the ears was shaved and disinfected, followed by making a small incision on the ear skin to confirm the location of auricular central artery. After the targeted artery was identified, a puncturing needle (22-Gauge) was inserted into the artery. Subsequently, the MS suspended in glycerol (20 mg/mL) were infused slowly, from the positioned proximal to the distal artery. The rabbits treated intra-arterially with glycerol alone were set as the control. After the embolization process was completed, the catheter was removed, and the injection site was pressed 15 min to stop bleeding. The rabbits were further intramuscularly injected with antibiotics to prevent infection. At 0, 7, and 15 days post-embolization, the changes in the shape and color of the rabbit ears were inspected and photographed.

2.9 Histological examination of tissue damage

After embolization for 7 and 15 days, the ear tissues injected with glycerol and MS were carefully dissected, harvested, and fixed with 4% (w/v) paraformaldehyde solution for over two days. Afterward, the tissues were cut into small blocks and embedded in paraffin, then cut into longitudinal sections (5 µm). The specimens were stained with hematoxylin-eosin (H&E) and Masson's trichrome, followed by examination under an optical microscope to assess the embolization effect.

2.10 Ultrastructural findings of morphological changes in the vascular endothelial cells

At 15 days, the changes in the vascular ultrastructure treated with different formulations were examined. Briefly, the vascular segments in the embolized region were isolated from the crude ear tissue and trimmed into 1 mm^3 blocks. Subsequently, these tissues were fixed in 2.5 wt% GA in PBS

for approximately 24 h, followed by immersion in 1% osmium tetroxide for 4 h, and proceeded by dehydration with gradient ethanol. The tissues were then embedded in epoxy resin (Epon 812) and cut into ultrathin sections (1 μm). Thereafter, the specimens were stained with uranyl acetate and lead citrate. Finally, the sections were observed under a Hitachi HT7700 transmission electron microscopy (TEM, Hitachi, Japan) to evaluate the morphological changes in the vascular endothelial cells.

2.11 Statistical analysis

All results obtained were analyzed by student's *t*-test (SPSS 22.0, IBM, Armonk, USA). The statistical significant difference was indicated with $*P < 0.05$ or $**P < 0.01$.

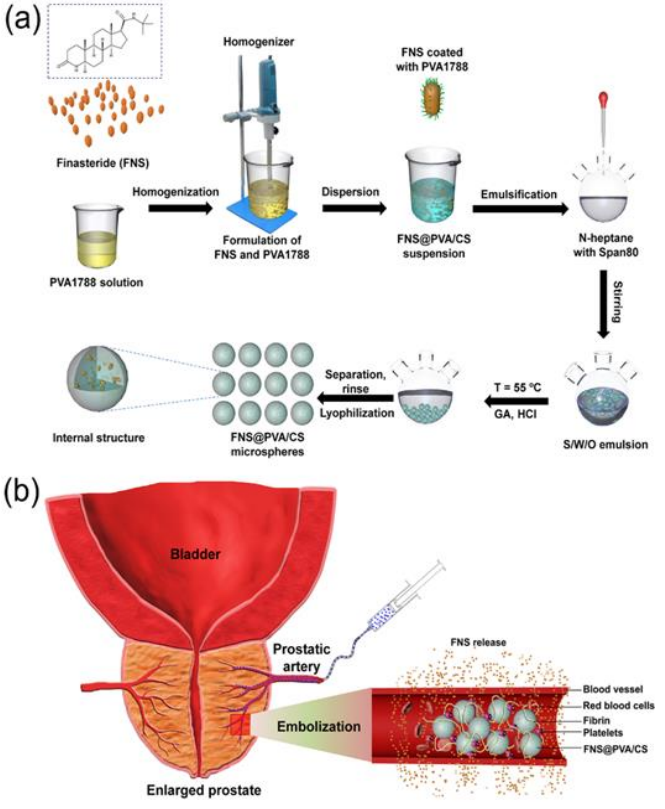

Fig. 1 Schematic illustration of (a) the preparation process of FNS@PVA/CS MS using a combination strategy of homogenization and S/W/O emulsification crosslinking method, and (b) the prepared FNS@PVA/CS MS for the treatment of BPH.

3. Results and discussion

3.1 Preparation and morphological characterization of prepared MS

Fig. 1 illustrates the preparation process of the FNS@PVA/CS MS by a modified S/W/O emulsification crosslinking method aiming at PAE for BPH therapy. The surface morphology, internal structure, and size distribution of drug-free and drug-loaded PVA/CS MS, as well as the morphological properties of the drug crystals are presented in Fig. 2. As shown in Fig. 2a1 and a2, the pure FNS crystals are in a form of polyhedron-shape and elongated structure, the size of most crystals is in the range of 5-200 μm and with small granules on the surface. The optical microscopic images (Fig. 2b1, c1) and FESEM images (Fig. 2b2, c2) show that both PVA/CS and FNS@PVA/CS MS are homogeneously distributed, perfectly spherical, and well-dispersed. At higher magnification, as illustrated in Fig. 2b3, the blank PVA/CS MS possess a continuous smooth surface, whereas the FNS@PVA/CS MS appear to present a rough surface, which could be attributed to the solid drug crystals embedded near the surface of MS (Fig. 2c3). Moreover, the cross-sections of PVA/CS MS show that they are comprised of compact and dense substance with visible pores (Fig. 2b4), which could be due to the formation of gas bubbles during the preparation of MS. For FNS@PVA/CS MS, it is clear that the drug microcrystals are incorporated into the microcavities of the MS (Fig. 2c4) (indicated by yellow arrows). The mean particle sizes of PVA/CS and FNS@PVA/CS MS are found to be 188.9 and 191.5 μm, respectively (Fig. 2d, e), indicating their suitability for following *in vivo* embolization.

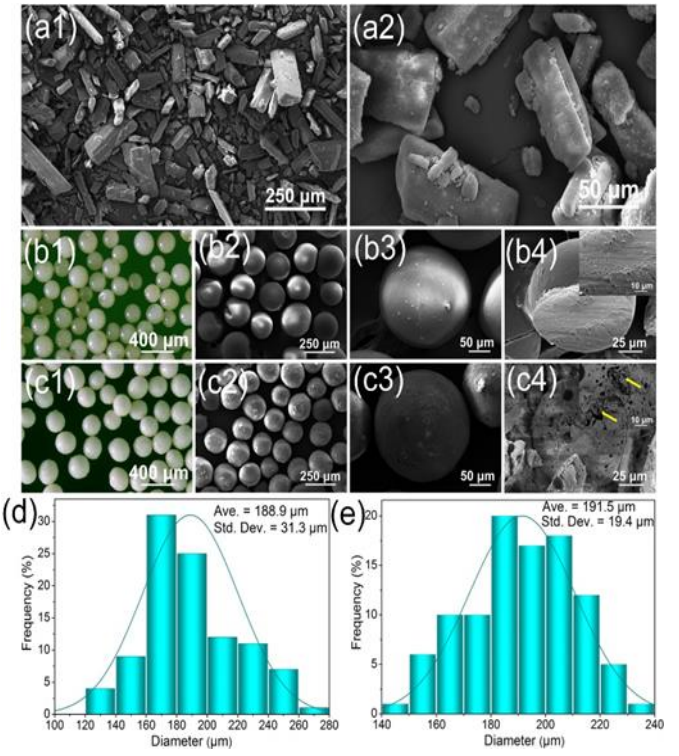

Fig. 2 FESEM images of (a1) pure FNS crystals and the surface morphology at higher magnification (a2). (b1) and (c1) show the optical micrographs of PVA/CS and FNS@PVA/CS MS. (b2) and (c2) display the FESEM images of the surfaces of PVA/CS and FNS@PVA/CS MS at low magnification, while (b3) and (c3) are the corresponding magnified images of (b2) and (c2). (b4) and (c4) present the FESEM images of the cross-sections of PVA/CS and FNS@PVA/CS MS, the insets are the corresponding magnified images. (d) and (e) display the size distribution results of PVA/CS and FNS@PVA/CS MS, respectively.

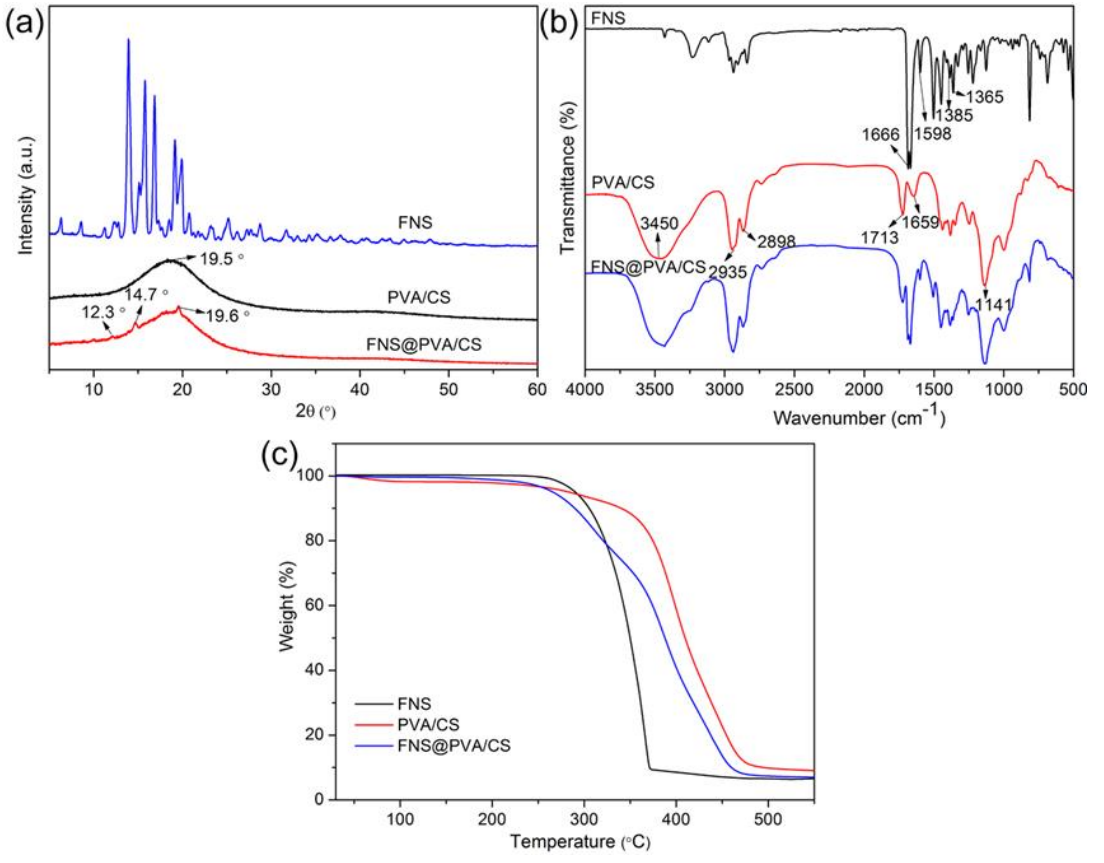

Fig. 3 Representative XRD pattern (a), FTIR spectra (b), and TGA curves (c) of pure FNS, placebo PVA/CS and FNS@PVA/CS MS.

Considering the immiscibility of hydrophobic drug in the hydrophilic PVA/CS polymeric matrix, it would lead to the precipitation in the outer phase when encapsulating the solid drug crystals directly in the PVA/CS through the traditional S/W/O method. Previously, Zhang *et al*. employed the sonicator and homogenizer to break the entecavir (ETV) crystals into pieces and encapsulated the drug into the MS using the S/O/W spraying method, which greatly increased the drug encapsulation efficiency and drug loading content.[36] In another study, Umemoto and his co-workers verified that the surfactant could significantly increase the wettability of the hydrophobic drug, which contributed to the enhancement of drug solubility.[37] In the present study, the homogenization technique was used to obtain the desired final size of the drug crystals, which resulted in an increased specific surface area and facilitated the wetting of the drug crystal surface. At the same time, the drug crystals were dispersed in the PVA1788 solution, which acted as an effective surfactant due to its amphiphilic nature. In fact, the PVA molecule has a hydrophobic chain and a hydrophilic end group, the hydrophobic chains occupy space at the solid-liquid interface, while the hydrophilic end groups are extended in the outer aqueous phase. Thus, the steric hindrance and increase in the energy barrier would prevent the aggregation of the crystals.[38] In addition, the adsorption of surfactant onto the FNS crystal surface reduced the solid/liquid interfacial tension, which could improve the wetting of the hydrophobic drug and thus, increase the affinity to the PVA/CS polymeric matrix. Thereby, the presence of surfactant on the drug surface made the hydrophobic drug wettable and was beneficial for the FNS to be encapsulated within the PVA/CS matrix.

3.2 Physicochemical characterizations

The XRD patterns recorded for the FNS, PVA/CS, and FNS@PVA/CS MS are displayed in Fig. 3a. The pure drug exhibited intense characteristic peaks due to its high crystalline nature. The XRD pattern of PVA/CS MS showed an evidenced peak at 19.5º, suggesting its semi-crystalline structure, which was mainly ascribed to the intermolecular hydrogen bonds formation in the polymer. After encapsulation of FNS in the polymeric MS, the presence of the drug in the MS was evidenced by well-resolved XRD peaks at 2θ of 12.3º, 14.7º, and 19.6º compared to the drug-free MS, indicating that the FNS retained its crystalline form in the polymeric matrix.

The encapsulation of FNS within the PVA/CS polymeric MS as well as the drug-polymer interaction was further confirmed by FTIR analysis. As presented in Fig. 3b, the pure FNS showed its characteristic peaks at 1666 and 1598 cm^{-1}, which were due to the two amide groups, whereas the peaks observed at 1385/1365 cm^{-1} corresponded to the tert-butyl group.[39] In the case of PVA/CS MS, a broad peak presented at 3450 cm^{-1} was assigned to the -OH stretching vibration of absorbed water moisture. The main absorption peak presented at 1141 cm^{-1} corresponded to the C-O stretching vibration of ester groups after crosslinking.[40] The intense peaks appeared at 1713 and 1659 cm^{-1} were owing to the C=O and C=C

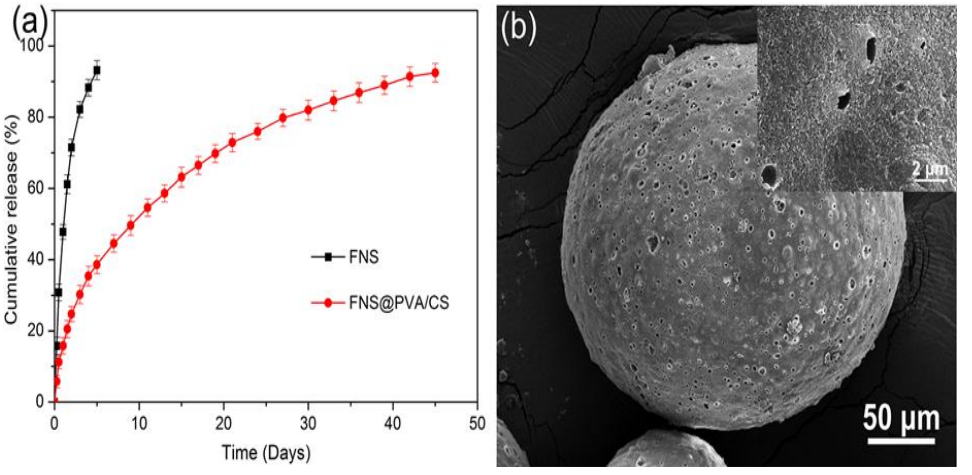

Fig. 4 (a) Release profiles of pure FNS and FNS@PVA/CS MS at different time points performed in PBS at 37 ºC (n = 3, pH = 7.4). (b) FESEM images of FNS@PVA/CS MS after 45 days of release in PBS, the inset image shows the surface morphology at higher magnification.

stretching vibration, respectively.[41] Additionally, the presence of intense peaks at 2935 and 2898 cm^{-1} were assigned to the CH_2 vibrational stretching.[42] The absorption peaks related to CS did not appear in the drug-free or drug-loaded PVA/CS MS, which could be due to the low sensitivity of FTIR to detect the functional groups (*i.e.*, NH_2) as a result of the small amount of CS in the MS formulations. Notably, the characteristic peaks in the FTIR spectrum of FNS@PVA/CS MS were similar to those of PVA/CS MS. Besides, the new peaks of the drug were also observed in the drug-loaded MS. It indicated that the main characteristic peaks of the drug were reflected in the FNS@PVA/CS MS, without new chemical bonds formed, disappeared, or shifted. These results confirmed the validity of the modified S/W/O emulsification crosslinking method to encapsulate the hydrophobic FNS into the PVA/CS polymer matrix, and there were no chemical interactions occurred between the FNS and PVA/CS.

The thermal characteristics of FNS, PVA/CS, and FNS@PVA/CS MS were investigated *via* TGA analysis. As presented in Fig. 3c, the FNS exhibited one step of weight loss covering the temperature range of about 250 to 372 ºC, which corresponded to the thermal degradation of the drug. With regard to the TGA thermogram of PVA/CS MS, two steps of weight loss were observed, where the first step covered the temperature range of about 30 to 200 ºC could be as a result of the evaporation of adsorbed water, while the second step covered the temperature range of about 200 to 480 ºC corresponded to the thermal degradation of PVA/CS. In the TGA thermogram of FNS@PVA/CS MS, the slight weight loss between 30 to 200 ºC was the same as PVA/CS MS, whereas a moderate weight loss between 200 to 345 ºC was attributed to the decomposition of FNS. In addition, the main thermal decomposition temperature shifted slightly towards the lower temperature range than that of PVA/CS MS, which might be due to the presence of FNS in the PVA/CS resulted in lower thermal degradation temperature for the drug-loaded MS. Furthermore, the drug-loaded MS showed a significant weight loss from 345 to 480 °C, indicating the thermal decomposition of PVA/CS polymeric matrix. Based on the TGA results, both MS prepared in our study showed excellent thermal stability, and could be used for embolization applications.

3.3 *In vitro* release of FNS from FNS@PVA/CS MS

The actual DL and EE for FNS@PVA/CS MS, determined quantitatively by an extraction method, were calculated to be 12.5% and 62.5%, respectively. During the preparation of drug-loaded MS *via* inverse emulsification crosslinking method, there exist many factors that affect the EE of the drug in a drug delivery system.[43] Specifically, the affinity between the drug and polymers play an important role in drug encapsulation into the MS. In the present study, the hydrophobic FNS was immiscible with the hydrophilic PVA/CS polymeric matrix to form a stable emulsion due to the significant difference in hydrophobicity. To address this problem, the modified S/W/O emulsification crosslinking method was employed, where the solid drug dispersion with improved wetting was formulated and well dispersed in the polymeric matrix, thus enhancing the drug loading capacity. The cumulative FNS release profiles obtained for the pure FNS and FNS@PVA/CS MS are depicted in Fig. 4a. According to the results, the free drug exhibited a quite high release rate, with approximately 47.8 % of the drug being released within 24 h and 93.2 % of the drug was released on day 5, which indicated an apparent diffusion-controlled release manner. For FNS@PVA/CS MS, the drug release profile demonstrated a high initial release rate followed by a near-linear release profile for over 45 days. Considering that a portion of encapsulated micronized FNS crystals were unevenly distributed near the surface of MS, thus facilitating the release medium to penetrate into the surface layer of the MS and allowed the drug to be released in the outer release medium, thus leading to the initial rapid drug release. The following sustained drug release may be associated with the

dense polymeric matrix that could delay the medium penetration and impede the diffusion of FNS to some extent, which would guarantee sufficient drug release at the prolonged stage. Although the slow degradation of CS may generate small pores on the MS, the sustained and prolonged drug release was achieved, which might be due to the fact that the hydrophobic drug is slow in water uptake and the low solubility of FNS may result in weak driving force (*i.e.*, the concentration difference of the drug between the MS and the outer release medium). Fig. 4b showed that the rough and porous surface structure of FNS@PVA/CS MS was formed after 45 days release in PBS, from which the dissolved drug was diffused into the release medium. Taken together, the modified S/O/W emulsification crosslinking method improved the hydrophobic FNS encapsulation into PVA/CS and achieved a sustained drug release in a prolonged manner.

To date, various polymeric drug delivery systems based on PVA and CS have been developed for embolotherapy owing to their excellent biocompatibility and nontoxicity, which combined the mechanical embolization of the target tissue and simultaneously delivery of the chemotherapeutics.[44-48] The anticancer drugs such as DOX and irinotecan (Iri) are usually loaded into the polymeric MS by ionic interactions or emulsification crosslinking method. For example, Ashrafi *et al*. prepared the PVA-2-acrylamido-2-methylpropane sulfonic acid (AMPS) beads (DC bead), the introduction of sulfonic acid groups on the polymer allowed the DOX and Iri loading into the beads through ionic interactions.[49] Park *et al*. prepared the DOX-loaded CS MS by emulsification crosslinking method, the drug loading and release behaviors could be adjusted by changing the concentration of tripolyphosphate (TPP) and the crosslinking time. *In vivo* embolization in a rabbit auricle model demonstrated that the DOX-loaded CS MS could be used as a potential anticancer embolic agent as it showed prominent antitumor activity against VX2 cells.[50] Although the available drug-loading methods for these hydrophilic PVA and CS polymers are effective to load the hydrophilic drug, these may not be suitable to load the hydrophobic drug due to the inherent incompatibility of the hydrophilic polymer network and the hydrophobic drug. Recently, Zhang *et al*. used the bleomycin-eluting HepaSphere MS to treat BPH in a canine model. The hydrophilic bleomycin was loaded into the HepaSphere MS by a swelling method, *in vitro* drug release study showed that the drug-loaded HepaSphere MS exhibited burst release within 1 h, followed by a sustained release pattern, with 57.3% of bleomycin released within 7 days.[5] In the present study, the FNS crystals were successfully loaded into the PVA/CS polymeric matrix through the modified S/W/O emulsification crosslinking method, which showed improved drug-loading and sustained drug release up to 45 days. The prepared FNS@PVA/CS MS in this study was originally to load the hydrophobic FNS in a hydrophilic polymeric matrix. Therefore, the newly developed FNS@PVA/CS MS could be used as a promising long-term sustained release system for BPH embolotherapy.

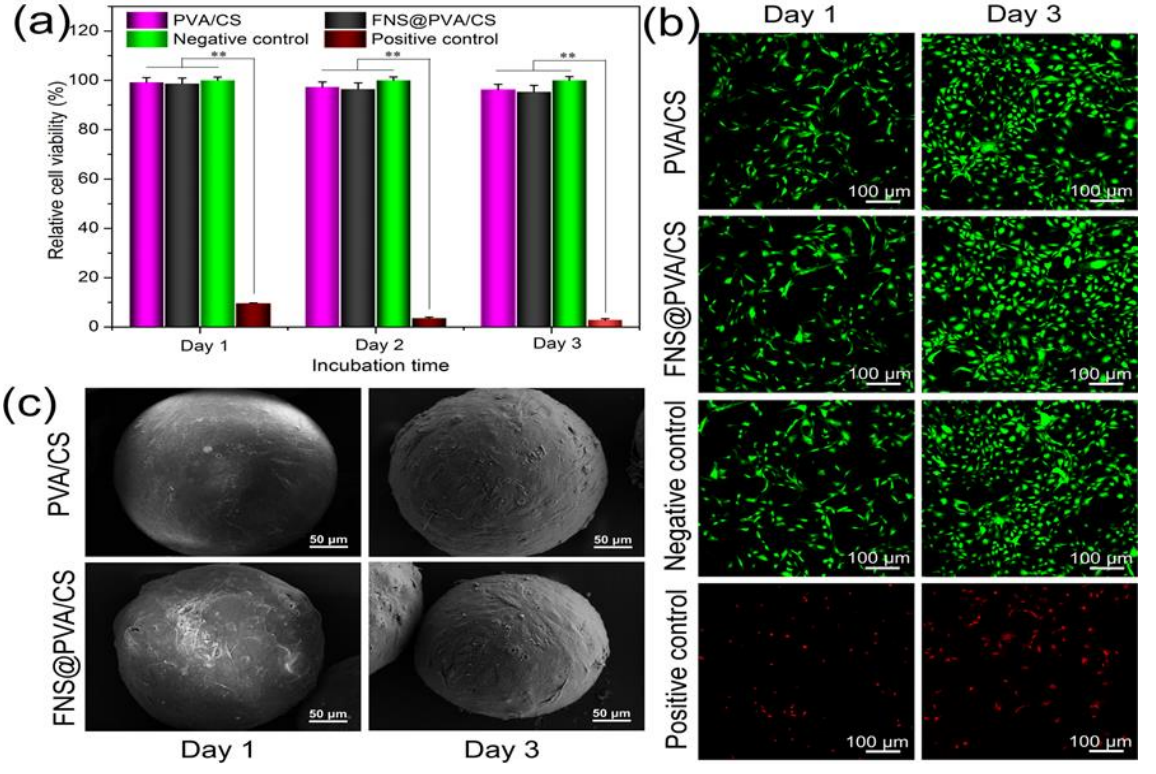

Fig. 5 (a) Cell viability of HVSMCs incubated with PVA/CS and FNS@PVA/CS MS abstracts (10 mg/mL) for 1, 2, and 3 days (** $P < 0.01$, n = 5). (b) CLSM images of Live/Dead assays, which distinguishing the live (green) and dead (red) cells. (c) FESEM images of HVSMCs adhering on the PVA/CS and FNS@PVA/CS MS after 1 and 3 days of incubation.

3.4 Cytocompatibility of the PVA/CS and FNS@PVA/CS MS

Considering the MS should be safe when used as an embolic agent *in vivo*, while cytotoxicity evaluation is on the first lane for screening biocompatibility of new materials.[51,52] Therefore, the biosafety of the MS was evaluated based on CCK-8 assays, Live/Dead assays, and cell morphology on MS.

Fig. 5a shows the *in vitro* relative cell viability results of HVSMCs incubated with the MS extracts for different periods. It reveals that the cells in contact with the extracts of PVA/CS and FNS@PVA/CS MS had a relative cell viability of 99.2% and 98.7% on day 1, 97.3% and 96.4% on day 2. After 3 days, the relative cell viability reached 96.2% and 95.3%, respectively. There was no significant difference in the relative cell viability between the MS and negative control groups at all time points. It should also be noted that the relative cell viability in the positive control group showed much lower values in all evaluation periods, i.e., less than 10%, in comparison with the negative control and MS groups. These results indicated that the extracts of the tested MS had no cytotoxicity towards HVSMCs.

As a complementary study, the CLSM images of the cells co-cultured with the MS were also performed to determine the cytotoxicity, while the negative and positive control groups were also involved. As shown in Fig. 5b, it was observed that the HVSMCs co-cultured with MS for 1 day, the cells grew well and exhibited the natural morphology of spindle shape. In addition, the majority of the cells were viable (stained green) with almost no dead cells (stained red) were detected in the CLSM images. Similar staining patterns were observed in the negative control groups. After the incubation extended to 3 days, more viable cells could be observed to be densely distributed in the MS and negative control groups, indicating that the cells proliferated well in these groups. Moreover, the MS groups showed comparable viable cell numbers with the negative control groups on day1 and day3, indicating that the MS did not cause any cytotoxicity *in vitro*. In contrast, it was evident that the dead cells were distinguished in the positive control groups after 1 and 3 days of culture, the cells constrained into an abnormal morphology with a spheroidal shape and were poorly survived, which was associated with the potentially toxic effects towards the cells. These results were consistent with the CCK-8 results (Fig. 5a).

The cell adhesion on the biomaterials surface provided further evidence for demonstrating the biocompatibility.[53] Accordingly, the cell morphology on the MS surface is displayed in Fig. 5c. After 1 and 3 days of incubation, the cell adhesion efficiencies and morphologies on both PVA/CS and FNS@PVA/CS MS were similar. After 1 day, the cells were extensively adhered on the MS surface and spread out to maintain the physical contact with each other through filopodia. After extending the incubation for 3 days, the cell numbers on the MS surface increased and bridged with each other, tending to form a confluent dense cell layer to cover the surface of MS. Therefore, the MS exhibited excellent cytocompatibility for cell adhesion and proliferation, which is in agreement with the results of CCK-8 assays (Fig. 5a) and CLSM observations (Fig. 5b).

Based on the results above, it is suggested that the MS were favorable for HVSMCs proliferation and adhesion, which revealed their non-cytotoxicity nature and, as a consequence, the MS would be safe for *in vivo* embolization.

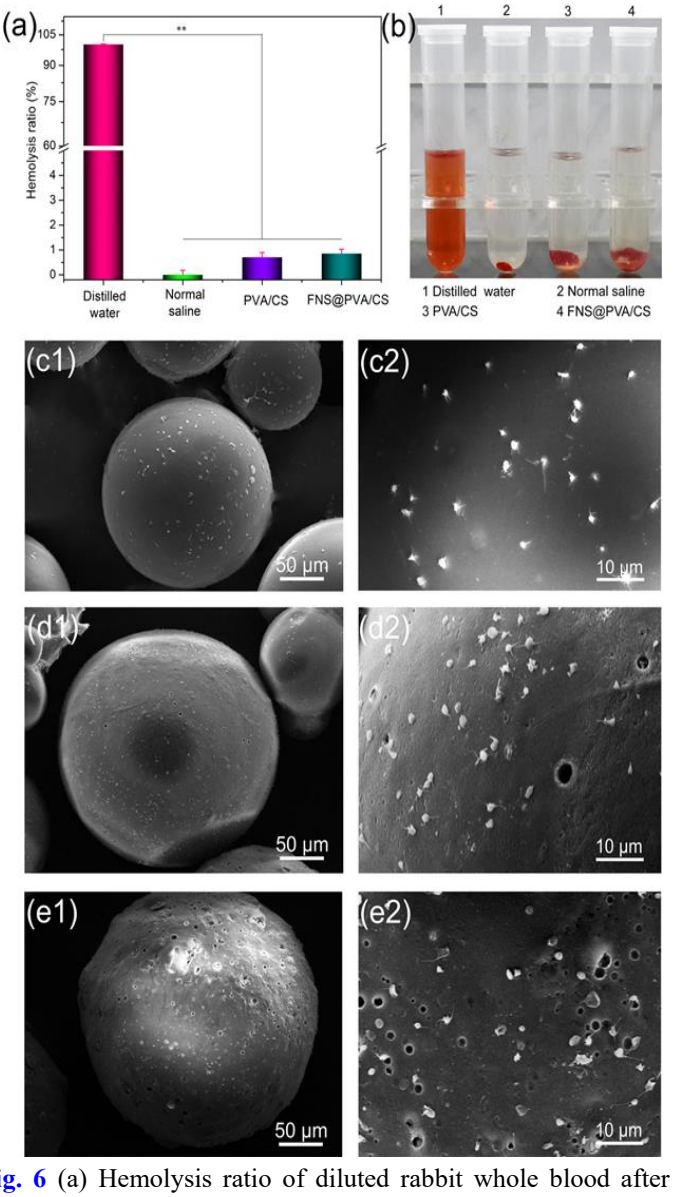

Fig. 6 (a) Hemolysis ratio of diluted rabbit whole blood after incubation with PVA/CS and FNS@PVA/CS MS at 37 ºC for 1 h. The distilled water and normal saline were used as the positive and negative control, respectively. (**$p < 0.01$, n = 5). (b) Visual observations of hemolysis. (c1, c2), (d1, d2), and (e1, e2) are the FESEM images of platelets adhesion on the glass, PVA/CS, and FNS@PVA/CS MS, respectively.

3.5 Hemocompatibility of the PVA/CS and FNS@PVA/CS MS

The hemocompatibility is one of the main concerns in the newly developed embolic agents as they directly contact with the blood.[54] The hemolysis was measured quantitatively and

the results are shown in Fig. 6a. The hemolysis ratio of the positive (distilled water) and negative control (normal saline) groups were set as 100% and 0%, respectively. The PVA/CS and FNS@PVA/CS MS showed similar hemolytic activity compared to the negative control, where the hemolytic values for PVA/CS and FNS@PVA/CS MS were found to be 0.70% and 0.85%, respectively, which were lower than 2% and considered to be non-hemolytic.[55] This was further confirmed by the macroscopic image shown in Fig. 6b, it revealed that the distilled water treated diluted blood induced leakage of hemoglobin, while there was no obvious hemoglobin release could be discerned in the negative and MS groups. These results revealed that the MS exhibited no obvious hemolytic effects.

Platelet adhesion and activation experiments are also important methods to ascertain the hemocompatibility of a material.[56] Fig. 6c1-e2 show the typical FESEM images of the platelets adhesion on the MS. It is clear that the PVA/CS (Fig. 6d1, d2) and FNS@PVA/CS (Fig. 6e1, e2) MS experienced similar levels of platelets adhesion. The platelets were sparsely scattered on the MS surface, showing that most platelets were nearly round with minimal dendritic extension. This result suggested that the adhered platelets were in a low degree of activation.[57] Whereas on the glass MS (Fig. 6c1, c2), numerous platelets adhered on the MS surface. In addition, the MS surface exhibited severe activation of platelets with mostly deformed and elongated pseudopodia, which would eventually induce the formation of more platelets aggregation and thrombus formation.[58] Collectively, these results demonstrated that the PVA/CS and FNS@PVA/CS MS showed good performance in hemocompatibility and could be safe for *in vivo* applications.

3.6 Macroscopic observations of changes in the appearance of rabbit ears

The *in vivo* embolization efficacies of the MS were investigated by assessing the ear skin changes in a rabbit ear model, owing to its easy establishment, inspection, and low cost.[33,59,60] The glycerol solution was used as a control for comparison. As displayed in Fig. 7, after injection of the solution into the auricular central artery, the macroscopic appearance of the ears remained in a normal state throughout the entire embolization period, which might be due to the glycerol was flowed away with the blood stream. However, the progressive ear skin color changes and ischemic necrosis were observed during the embolization in the MS groups. As seen in the macroscopic image, after embolization with PVA/CS and FNS@PVA/CS MS, the distal ear vessel immediately became pale, which confirmed that the MS effectively obstructed the blood flow in the blood vessels. After 7 days of embolization, the ear tissue along the auricular central artery appeared dark blue, indicating a small area of skin necrosis occurred in the rabbits. On day 15, large areas of blackened ear skin were evidenced, implying that almost total ears had pronounced necrosis. Overall, these findings suggested that the MS could effectively occlude the vascular lumen and induce the irreversible ischemic necrosis near the embolized vessels.

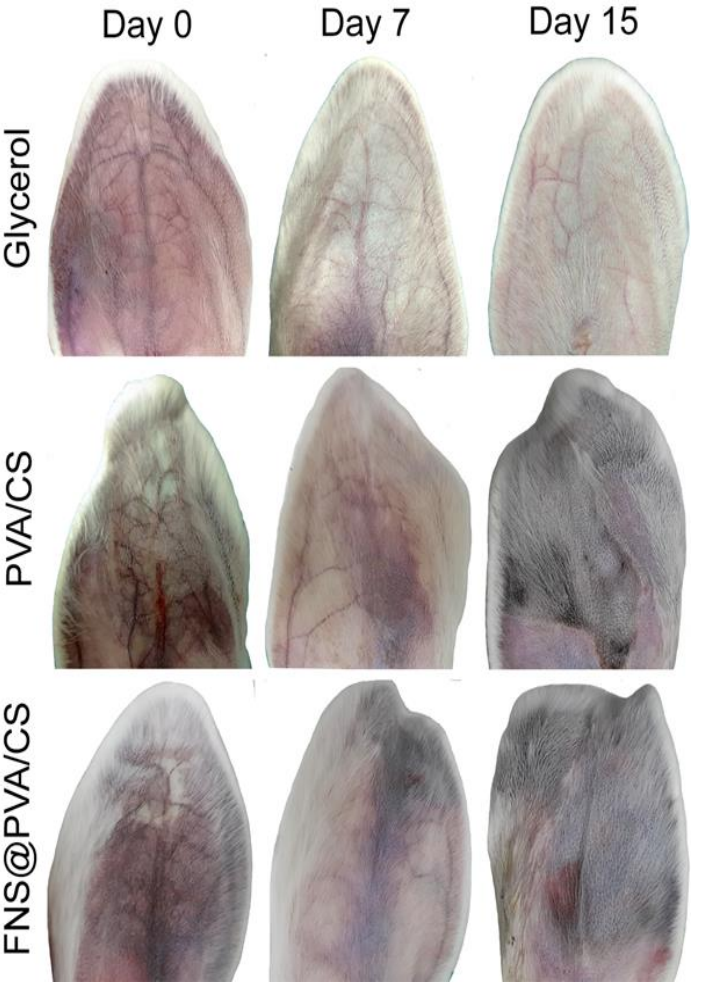

Fig. 7 The macroscopic observations of the rabbit ear changes after treatment with glycerol, PVA/CS, and FNS@PVA/CS MS for 0, 7, and 15 days.

3.7 Histopathological changes in the ear tissues

To further assess the embolization efficacy and tissue compatibility of the MS, the histological detection was performed *via* H&E staining at 7 and 15 days after embolization. Fig. 8a shows the representative micrographs of the longitudinal sections of ear arteries. Apparently, in the glycerol injection group, the erythrocytes were identified to form thrombus inside the arteries, with no obvious inflammatory reactions in the periphery of the embolic arteries after 7 and 15 days upon injection of the glycerol. Conversely, the auricular embolization with PVA/CS and FNS@PVA/CS MS indicated that the erythrocytes coagulated with the MS and filled in the arteries, thus avoiding the migration of MS

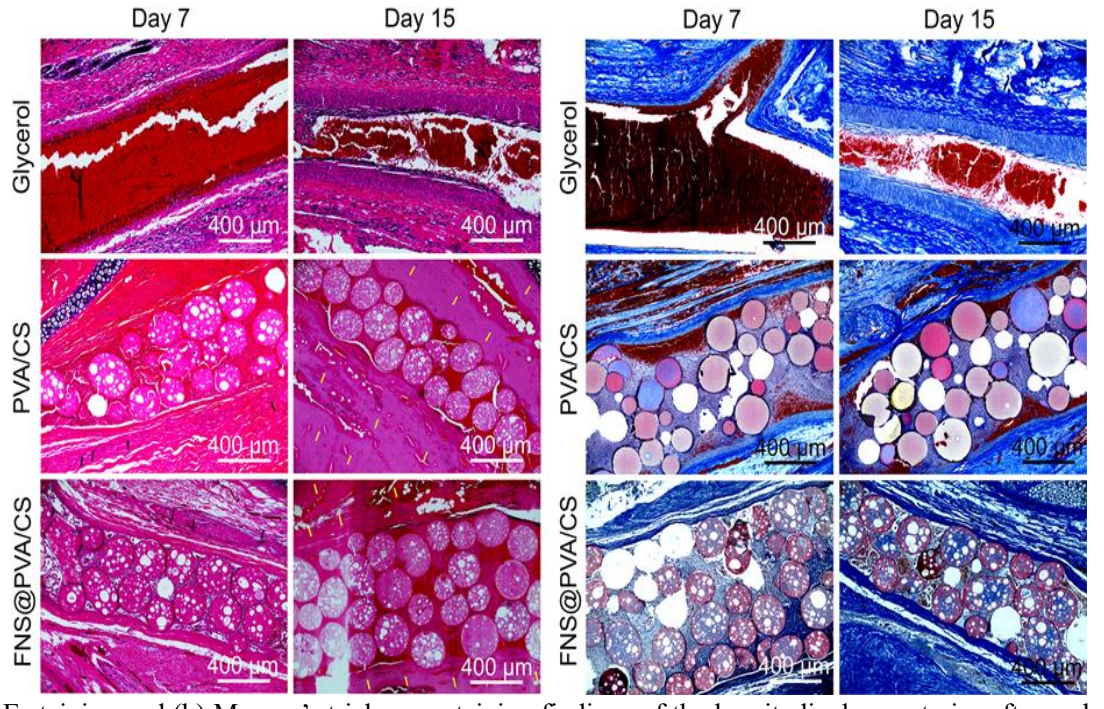

Fig. 8 (a) H&E staining and (b) Masson's trichrome staining findings of the longitudinal ear arteries after embolization with glycerol, PVA/CS, and FNS@PVA/CS MS for 7 and 15 days. The black arrows in (a) present the moderate inflammatory cells infiltration around the implants, while yellow arrows present the fibrotic necrosis in the perivascular parenchyma of the ears.

and occluding the blood flow persistently. On day 7, it revealed that the segmental ischemic necrotic lesions were observed in the perivascular parenchyma. In addition, a moderate degree of inflammatory reactions, mainly lymphocytes and neutrophils infiltration (black arrows), could be observed around the periphery of the embolized arteries. With the embolization prolonged to 15 days, the inflammatory reactions were alleviated, and the fibrotic necrosis was more evident in the ear tissues (yellow arrows). These results indicated that the MS showed good compatibility with the blood vessels and could effectively cut off the blood supply of the ear arteries for over 15 days, and eventually brought about ischemic necrosis of the ear tissues.

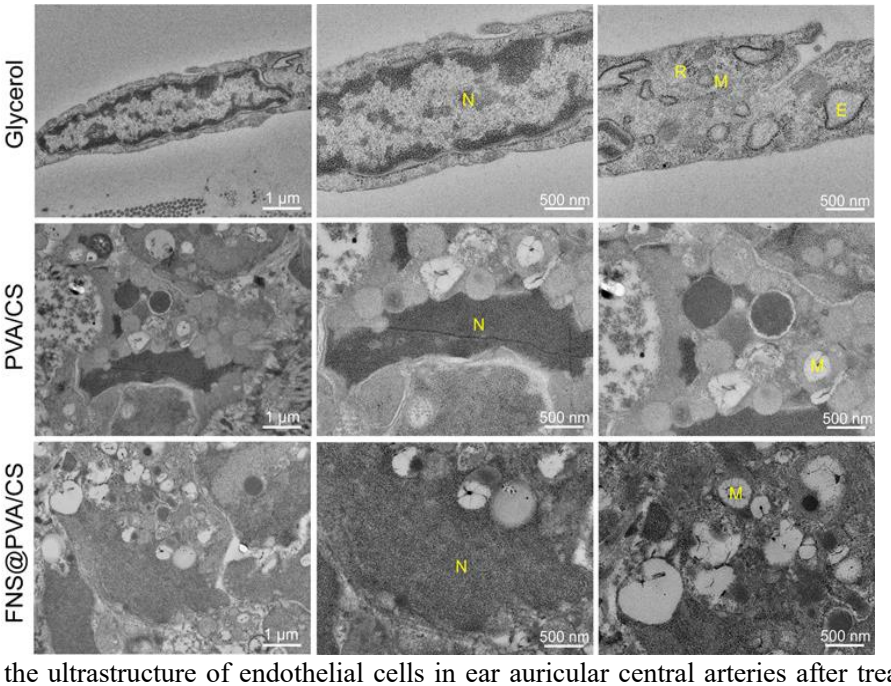

Fig. 9 TEM images of the ultrastructure of endothelial cells in ear auricular central arteries after treatments with glycerol, PVA/CS and FNS@PVA/CS MS for 15 days. The endothelial cells retained their integrity in the glycerol-treated group, while there was some severe abnormality of the endothelial cells induced by the ischemic injury in the PVA/CS and FNS@PVA/CS MS treated groups. [Nucleus (N); Ribosome (R); Endoplasmic reticulum (E); Mitochondria (M)]

To better understand the short- and long-term ischemic necrosis induced by the MS, the tissue sections were stained with Masson's trichrome staining. As depicted in Fig. 8b, there was an absence of collagenous formation in the histologic tissue sections after treatment with glycerol for 7 and 15 days, indicating no ischemic changes were observed, which was due to the diffusion of glycerol with the blood and could not cause the blockage of blood vessels. In contrast, there were associated incidences of ischemic complications in the PVA/CS and FNS@PVA/CS MS groups over the whole course of this study. At 7 days after embolization, the microscopic observations revealed some portions of the perivascular tissues were replaced by fibrosis, on which the collagen deposition was evidenced along the peripheral regions of arteries. On day 15, the acute ischemic changes with more dense fibrotic tissue deposition were observed, revealing that more extensive infarction occurred in the ear parenchyma owing to the persistent occlusion of the ear arteries. Although we attempted to provide the long-term embolization effects, the extended embolization with the MS would lead to drying of the necrotic ears and eventually separated from the ears. The microscopic examinations suggested that the treatments by the MS could result in progressive fibrosis, and could be used as for effective embolization.

3.8 Effects of ischemia on the ultrastructure of endothelial cells

For the purpose of investigating the morphological alternations in vascular ultrastructure after treatments with glycerol, PVA/CS and FNS@PVA/CS MS for 15 days, the endothelial cells of rabbit ear arteries were studied by TEM. As illustrated in Fig. 9, the endothelial cells showed normal appearance in the glycerol group, where degenerative and necrotic changes did not occur according to the TEM observations. However, in the PVA/CS and FNS@PVA/CS MS groups, the effect of ischemia on the ultrastructural changes was obvious. It should be noted that the nucleus and cytoplasm had thorough disintegrative necrosis, which includes pleomorphic and degenerating nucleus with indistinct nuclear membrane, mitochonadrial swelling and misshapen, depletion of cytoplasmic organelles as well as cytoplasmic vacuolation, indicating extensive damage to the endothelial cells. These findings suggested that the severe ischemic necrosis, induced by the persistent embolization in the MS-treated rabbits, could result in prominent ultrastructural alternations of endothelial cells, which would lead to decreased blood perfusion in the ear parenchyma and continuous hypoxia due to the impairment in the endothelial permeability.[61]

4. Conclusions

In this study, the micronized FNS crystal suspension was first obtained through a homogenization technique in the presence of a hydrophilic surfactant, followed by the S/W/O emulsification crosslinking method to encapsulate the FNS in the PVA/CS MS matrix. The addition of a small amount of PVA1788 improved the wetting of the drug and minimized the agglomeration, and thus improved its affinity to the polymeric matrix. The as-prepared FNS@PVA/CS MS were monodispersed with a mean particle size of 191.5 μm. The drug retained its crystalline state in the MS, which acted as a drug reservoir for controlled and sustained release up to 45 days. The biological evaluations showed excellent cytocompatibility and hemocompatibility of the MS. Additionally, the gross inspection and histopathology analysis in a rabbit ear embolization model verified the progressive ischemic necrosis on ears due to the vascular occlusion with the MS. Furthermore, the persistent embolization could lead to prominent ultrastructural alternations in the endothelial cells resulted from severe ischemic necrosis. All these results demonstrate that the newly developed FNS@PVA/CS MS could be used as a potential drug-delivering embolic agent and offer great promise for prolonged and localized delivery of FNS in PAE applications. Further studies will be performed on a beagle BPH model to determine the therapeutic efficacy of the MS.

Acknowledgements

This research was financially supported by the National Natural Science Foundation of China (Grant No. 21774039, 51973076) and the project of National Key Research and Development Program of China (2018YFE0123700).

Supporting Information

Not applicable

Conflict of interest

There are no conflicts to declare.

References

[1] P. Xiang, M. Wang, D. Guan, D. Liu, Y. Wang, Y. Hao, S. Li, Y. Liu and H. Ping, *Eur. Urol. Open Sci.*, 2020, **19**, 3-15, doi: 10.1016/j.euros.2020.05.001.

[2] V. Zumstein, P. Betschart, M. W. Vetterlein, L. A. Kluth, L. Hechelhammer, L. Mordasini, D. S. Engeler, T. M. Kessler, H. P. Schemid and D. Abt, *Eur. Urol. Focus*, 2019, **5**, 1091-1100, doi: 10.1016/j.euf.2018.09.005.

[3] F. C. Carnevale, A. M. Moreira, A. M. de Assis, A. A. Antunes, V. C. de Paula Rodrigues, M. Srougi and G. G. Cerri, *Radiology*, 2020, **296**, 191249, doi: 10.1148/radiol.2020191249.

[4] M. Kuang, A. Vu and S. Athreya, *Cardiovasc. Intervent. Radiol.*, 2017, **40**, 655-663, doi: 10.1007/s00270-016-1539-3.

[5] J. Zhang, B. Yuan, M. Wang, J. Fu, F. Duan, T. Wang, L. Shen, Y. Wang, J. Liu, Y. Shen, X. Wang, H. Zhang, H. Li, J. Yan and Z. Song, *J. Vasc. Interv. Radiol.*, 2020, **31**, 820-830, doi: 10.1016/j.jvir.2019.11.028.

[6] R. Ayyagari, T. Powell, L. Staib, J. Chapiro, A. Raja, S. Bhatia, T. Chai, S. Schoenberger and R. Devito, *J. Vasc. Interv. Radiol.*,

2020, **31**, 99-107, doi: 10.1016/j.jvir.2019.08.005.
[7] J. H. Hwang, S. W. Park, I. S. Chang, S. I. Jung, H. J. Jeon, Y. S. Lho, H. G. Kim, S. H. Paick and H. K. Park, *Biomed. Res. Int*., 2017, **2017**, 8732351, doi: 10.1155/2017. 8732351.
[8] T. Bilhim, J. Pisco, J. A. Pereira, N. V. Costa, L. Fernandes, L. C. Pinheiro, M. Duarte and A. G. Oliveira, *Radiology*, 2016, **281**, 289-300, doi: 10.1148/radiol.2016152292.
[9] J. B. Spies, S. Allison, P. Flick, M. McCullough, K. Sterbis, M. Cramp, J. B. DO and R. Jha, *J. Vasc. Interv. Radiol*., 2004, **15**, 793-800, doi: 10.1097/01.RVI.0000136982.42548.5D.
[10] Y. M. Nouri, J. H. Kim, H. K. Yoon, H. K. Ko, J. H. Shin and D. I. Gwon, *Korea J. Radiol*., 2019, **20**, 34-49, doi: 10.2214/AJR.19.21669.
[11] P. Popovic, B. Stabuc, R. Jansa and M. Garbajs, *Radiol. Oncol*., 2016, **50**, 418-426, doi: 10.1515/raon-2015-0045.
[12] Y. J. Kang, B. C. Lee, J. K. Kim, N. Y. Yim, H. O. Kim, S. B. Cho and Y. Y. Jeong, *Cardiovasc. Intervent. Radiol*., 2020, **43**, 55-64, doi: 10.1007/s00270-019-02349-9.
[13] K. Malagari, H. Moschouris, T. Kiakidis, S. Harward, A. Kelekis, S. Vrakas, D. Koundouras, D. Filipiadis, G. Glantzounis, E. Emmanouil, A. Chatziioannou, V. Vergadis, I. Elefsiniotis, J. Koskinas, S. Dourakis and N. Kelekis, *Cardiovasc. Intervent. Radiol*., 2019, **42**, 1551-1562, doi: 10.1007/s00270-019-02260-3.
[14] Y. Imai, M. Hirooka, Y. Koizumi, Y. Nakamura, T. Watanabe, O. Yoshida, Y. Tokumoto, E. Takeshita, M. Abe, H. Tanaka, M. Kurata, S. Kitazawa and Y. Hiasa, *Radiol. Case Reports*, 2017, **12**, 179-184,doi: 10.1016/j.radcr.2016.11.006.
[15] H. Xiang, L. Long, Y. Yao, Z. Fang, Z. Zhang and Y. Zhang, *Technol. Cancer Res. T.*, 2019, **18**, 1-12, doi : 10.1177/1533033819830751.
[16] Y. K. Lee, K. S. Jung, D. Y. Kim, J. Y. Choi, B. K. Kim, S. U. Kim, J. Y. Park, S. H. Ahn, K. H. Han, G. M. Kim, M. D. Kim and S. I. Park, *J. Gastroenterol. Hepatol*., 2017, **32**, 487-496,doi: 10.1111/jgh.13501.
[17] J. M. Pisco, T. Bilhim, L. C. Pinheiro, L. Fernandes, J. Pereira, N. V. Costa, M. Duarte and A. G. Oliveira, *J. Vasc. Interv. Radiol*., 2016, **27**, 1115-1122, doi: 10.1016/j.jvir.2016.04.001.
[18] A. Uflacker, Z. J. Haskal, T. Bilhim, J. Patrie, T. Huber and J. M. Pisco, *J. Vasc. Interv. Radiol*., 2016, **27**, 1686-1697, doi:10.1016/j.jvir.2016.08.004.
[19] J. M. Pisco, T. Bilhim, L. Pinheiro, L. Fernandes, J. A. Pereira, N. Costa, M. Duarte and A. Oliveira, *J. Vasc. Interv. Radiol*., 2015, **26**, S136-S137, doi: 10.1016/j.jvir.2014.12.366.
[20] Q. Liu, Y. Zhu, J. Liu, J. Qi and J. Kang, *Int. Urol. Nephrol*., 2017, **49**, 399-404,doi: 10.1007/s11255-016-1478-6.
[21] D. V. Neste, *Skin Res. Technol*., 2019, **25**, 712-719,doi: 10.1111/srt.12707.
[22] S. Kaushal and M. Sinha, *Word J. Pharm. Res*., 2015, **4**, 2393-2402.
[23] M. S. Irwig, *Sex. Med. Rev*., 2014, **2**, 24-35, doi: 10.1002/smrj.19.
[24] X. Li, X. Ji, K. Chen, M. W. Ullah, X. Yuan, Z. Lei, J. Cao, J. Xiao and G. Yang, *Biomater. Sci*., 2020, **8**, 2797-2813, doi: 10.1039/C9BM01775E.
[25] S. Minocha, S. Pahwa and V. Arora, *J. Biomed. Pharmaceut. Res*., 2019, **8**, 13-19, doi: 10.32553/jbpr.v8i1.565.
[26] A. Brunaugh and H. D. C. Smyth, *Drug Deliv and Transl. Re*., 2018, **8**, 1740-1750, doi: 10.1007/s13346-017-0444-x.
[27] M. Cerea, F. Pattarino, A. F. Bonda, L. Palugan and C. Vecchio, *Drug Dev. Ind. Pharm*., 2016, **42**, 1466-1475,doi: 10.3109/03639045.2016.1143953.
[28] J. Kluge, G. Muhrer and M. Mazzotti, *J. Supercrit. Fluid*, 2012, **66**, 380-388,doi: 10.3109/03639045.2016.1143953.
[29] S. Kamiya, M. Yamada, M. Washino and K. Nakashima, *Curr. Nanosci*., 2018, **14**, 143-147, doi: 10.2174/1573413713666171109155955.
[30] S. P. Chaudhari and R. P. Dugar, *J. Drug Deliv. Sci. Technol*., 2017, **41**, 68-77, doi: 10.1016/j.jddst.2017.06.010.
[31] Y. S. Lee, P. J. Johnson, P. T. Robbins and R. H. Bridson, *Eur. J. Pharm. Biopharm*., 2013, **83**, 168-173, doi: 10.1016/j.ejpb.2012.10.016.
[32] D. Peng, K. Huang, Y. Liu and S. Liu, *Int. J. Pharmaceut*., 2007, **342**, 82-86, doi: 10.1016/j.ijpharm.2007.05.002.
[33] X. Zhou, M. Kong, X. Cheng, C. Feng, J. Li, J. Li and X. Chen, *Carbohydr. Polym*., 2014, **113**, 304-313, doi: 10.1016/j.carbpol.2014.06.080.
[34] J. Li, X. Wu, Y. Wu, Z. Tang, X. Sun, M. Pan, Y. Chen, J. Li, R. Xiao, Z. Wang and H. Liu, *Mater. Sci. Eng. C*, 2017, **77**, 411-419, doi: 10.1016/j.msec.2017.03.276.
[35] M. F. Hsu, Y. S. Tyan, Y. C. Chien and M. W. Lee, *Sci. Rep*., 2018, **8**, 731, doi: 10.1038/s41598-018-19191-7.
[36] C. Zhang, A. Wang, H. Wang, M. Yan, R. Liang, X. He, F. Fu, H. Mu and K. Sun, *Int. J. Pharm*., 2019, **560**, 27-34, doi: 10.1016/j.ijpharm.2019.01.052.
[37] Y. Umemoto, S. Uchida, T. Yoshida, K. Shimada, H. Kojima, A. Takagi, S. Tanaka, Y. Kashiwagura and N. Namiki, *J. Drug Deliv. Sci. Technol*., 2020, **55**, 101401, doi: 10.1016/j.jddst.2019.101401.
[38] H. Takeuchi, H. Kojima, H. Yamamoto and Y. Kawashima, *J. Control Release*, 2001, **75**, 83-91, doi: 10.1016/S0168-3659(01)00368-6.
[39] T. A. Ahmed and K. M. El-say, *Eur. J. Pharm. Sci*., 2016, **88**, 246-256, doi: 10.1016/j.ejps.2016.03.015.
[40] J. Bergamasco, M. V. De Araujo, A. De Vasconcellos, R. A. Luizon Filho, R. R. Hatanaka, M. V. Giotto, D. A. G. Aranda and J. G. Nery, *Biomass Bioenerg*., 2013, **59**, 218-233,doi: 10.1016/j.biombioe.2013.09.006.
[41] E. A. Bary, A. Fekri and A. Harmal, *Int. J. Environ. Stud*.,

2018, **75**, 750-762, doi: 10.1080/10601325.2019.1593792.
[42] W. Zhang, Y. Ying, J. Ma, X. Guo, H. Huang, D. Liu and C. Zhong, *J. Membrane Sci.*, 2017, **527**, 8-17, doi: 10.1016/j.memsci.2017.01.001.
[43] N. V. N. Jyothi, P. M. Prasanna, S. N. Sakarkar, K. S. Prabha, P. S. Ramaiah and G. Y. Srawan, *J. Microencapsul.*, 2010, **27**, 187-197, doi: 10.3109/02652040903131301.
[44] C. L. Heaysman, G. J. Phillips, A. W. Lloyd and A. L. Lewis, *J. Mater. Sci: Mater. Med.*, 2016, **27**, 53, doi: 10.1007/s10856-015-5637-6.
[45] J. Namur, S. J. Citron, M. T. Sellers, M. H. Dupuis, M. Wa ssef, M. Manfait and A. Laurent, *J. Hepatol.*, 2011, **55**, 1332-1338, doi: 10.1016/j.jhep.2011.03.024.
[46] J. Namur, F. Pascale, N. Maeda, M. Sterba, S. H. Ghegediban, V. Verret, A. Paci, A. Seck, K. Osuga, M. Wassef, P. Reb and A. Laurent, *J. Vasc. Interv. Radiol.*, 2015, **26**, 1067-1075, doi: 10.1016/j.jvir.2015.03.014.
[47] L. Weng, P. Rostamzadeh, N. Nooryshokry, H. C. Le and J. Golzarian, *Acta Biomater.*, 2013, **9**, 6823-6833, doi: 10.1016/j.actbio.2013.02.017.
[48] L. Weng, H. C. Le, J. Lin and J. Golzarian, *Int. J. Pharm.*, 2011, **409**, 185-193,doi: 10.1016/j.ijpharm.2011.02.058.
[49] K. Ashrafi, Y. Tang, H. Britton, O. Domenge, D. Blino, A. J. Bushby, K. Shuturminska, M. den Hartog, A. Radaelli, A. H. Negussie, A. S. Mikhail, D. L. Woods, V. Krishnasamy, E. B. Levy, B. J. Wood, S. L. Willis, M. R. Dreher and A. L. Lewis, *J. Control. Release*, 2017, **250**, 36-47, doi: 10.1016/j.jconrel.2017.02.001.
[50] J. M. Park, S. Y. Lee, G. H. Lee, E. Y. Chung, K. M. Chang, B. K. Kwak, H. J. Kuh and J. Lee, *J. Microencapsul.*, 2012, **29**, 695-705, doi: 10.3109/02652048.2012.686526.
[51] S. Kehoe, N. Kilcup and D. Boyd, *Mater. Lett.*, 2012, **86**, 13-17,doi: 10.1016/j.matlet.2012.06.087.
[52] X. Liu, D. P. Rodeheaver, J. C. White, A. M. Wright, L. M. Walker, F. Zhang and S. A Shannon, *Regul. Toxicol. Pharm.*, 2018, **97**, 24-32, doi: 10.1016/j.yrtph.2018.06.003.
[53] M. Rahmati, E. A. Silva, J. E. Reseland, C. A. Heyward and H. J. Haugen, *Chem. Soc. Rev.*, 2020, **49**, 5178-5224, doi: 10.1039/D0CS00103A.
[54] M. Nalezinková, *Thromb. Res.*, 2020, **195**, 146-150, doi: 10.1016/j.thromres.2020.07.027.
[55] Standard practice for assessment of hemolytic properties of materials, Annual Book of ASTM Standards, ASTM F756-08, 2008.
[56] D. Zou, X. Luo, C. Han, J. Li, P. Yang, Q. Li and N. Huang, *Mater. Sci. Eng. C*, 2019, **96**, 509-521, doi: 10.1016/j.msec.2018.11.078.
[57] H. P. Felgueiras, L. M. Wang, K. F. Ren, M. M. Querido, Q. Jin, M. A. Barbosa, J. Ji and M. C. L. Martins, *ACS. Appl. Mater. Interfaces*, 2017, **9**, 7979-7989, doi: 10.1021/acsami.6b16415.
[58] T. Iba and J. H. Levy, *J. Thromb. Haemost.*, 2018, **16**, 231-241, doi: 10.1111/jth.13911.
[59] A. Momeni, E. M. Valliant, E. P. Brennan-Pierce, J. J. S. Shankar, R. Abraham, P. Colp and M. J. Filiaggi, *Acta Biomater.*, 2016, **32**, 286-297, doi: 10.1016/j.actbio.2015.12.012.
[60] Y. Zhuang, M. Yang and C. Liu, *Aesth. Plast. Surg.*, 2016, **40**, 421-427, doi: 10.1007/s00266-016-0630-0.
[61] T. A. Sutton, C. J. Fisher and B. A. Molitoris, *Kidney Int.*, 2002, **62**, 1539-1549, doi: 10.1046/j.1523-1755.2002.00631.x.

Author information

Xiaohong Li *is a postdoctoral research fellow at Shanghai Institute of Ceramics, Chinese Academy of Sciences. He received his Ph.D. degree in 2020 from Huazhong University of Science and Technology in biomaterials and tissue engineering. His research interests include development and evaluation of new multifunctional embolic agents, drug-loaded polymeric microspheres for tissue engineering, and functional nanomaterials for postoperative immunotherapy.*

Kun Chen *is a doctoral candidate in College of Life Science and Technology, Huazhong University of Science and Technology. He received his B.S. degree in mechanical engineering from Northwest Agricuture and Forest Science and Technology University. His current research is focused on the development of equipments for the preparation of biomedical hydrogel microspheres.*

Xiongfa Ji *is a postdoctoral research fellow at Guangdong Provincial People's Hospital. He received his Ph.D. degree from Department of Orthopaedic Surgery, Tongji Hospital, Tongji Medical College, Huazhong University of Science and Technology. His broad research interests include polymeric biomaterials, tissue engineering and bone tumor therapy.*

Xi Yuan *is a doctoral candidate in the Department of Orthopaedic Surgery, Tongji Hospital, Tongji Medical College, Huazhong University of Science and Technology. He received his B.S. degree in medicine from Nanchang University and M.S. degree in medicine from Huazhong University of Science and Technology. His current research is focused on nanomaterials, 3D printing, bone and cartilage regeneration.*

Zehua Lei *is a doctoral candidate in the Department of Orthopaedic Surgery, Tongji Hospital, Tongji Medical College, Huazhong University of Science and Technology. His broad research interests include osteoarthritis, cartilage repair and orthopedic biomaterials.*

Muhammad Wajid Ullah *is a Post-doctoral researcher at Huazhong University of Science and Technology. He obtained his B.S. and M.S. degrees from University of Peshawar and COMSATS University, respectively, and Ph.D. degree from Kyungpook National University. He has published >85 articles in peer reviewed international journals (h-index: >26). His research interests include the fabrication of bacterial cellulose and other natural polymers-based functional materials via 3D printing, advanced cell-free approach, and physico-chemical approaches for engineering of bone, skin, and other tissues as well as applications in drug delivery and biosensing.*

Jun Xiao *is a Professor, Doctoral supervisor at Huazhong University of Science and Technology, Director of the Department of Bone and Joint at Tongji Hospital. He received his Ph.D. degree from Tongji Medical College of Huazhong University of Science and Technology. He completed postdoctoral research at General Hospital of People's Liberation Army and his fellowship at the Massachusetts General Hospital, Harvard Medical School. His current research is focused on patient-customized implantation and treatment.*

Guang Yang *is Full Professor at Huazhong University of Science and Technology. She received Ph.D. degree in Chemistry from Wuhan University. She remained the Distinguished Young Chutian Scholar and Outstanding Talents in Hubei province, as well as Alexander von Humboldt and JSPS fellow. She has published more than 150 international papers, and applied more than 20 patents. Her current research is focused on the development of nanocellulose-based functional materials, design and fabrication of novel nano-drug transporters, 3D printing, nano-assembly of ordered materials, and tissue engineering.*

